

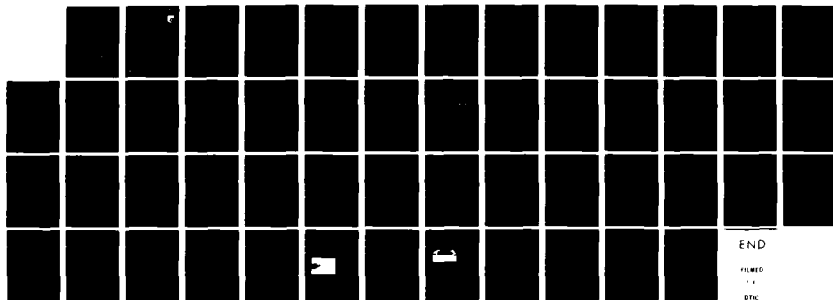
AD-A128 728

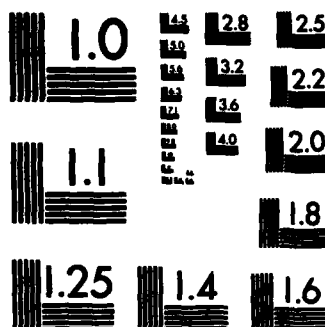
THALLIUM-DOPED SILICON INFRARED DETECTOR MATERIAL(U)
HONEYWELL INC BLOOMINGTON MN CORPORATE PHYSICAL
SCIENCES CENTER D E SCHAFER MAY 81 AFMAL-TR-88-4181
F33615-79-C-5847 F/G 17/5

1/1

UNCLASSIFIED

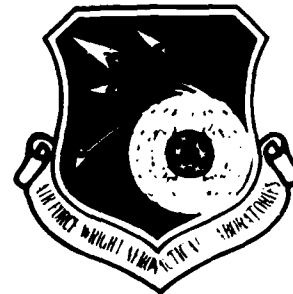
NL





AD A 120720

AFWAL-TR-80-4181



THALLIUM-DOPED SILICON INFRARED DETECTOR MATERIAL

Honeywell Inc.
Corporate Physical Sciences Center
10701 Lyndale Ave. S., Bloomington, MN 55420

May 1981

Technical Report AFWAL-TR-80-4181

Final Report for Period 1 June 1979 - 30 May 1980

Approved for public release; distribution unlimited.

MATERIALS LABORATORY
Air Force Wright Aeronautical Laboratories
Air Force Systems Command
Wright-Patterson Air Force Base, Ohio 45433

DTIC

50 OCT 20 1982

A

DTIC FILE COPY

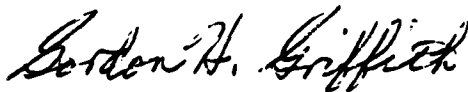
82 10 26 020

NOTICE

When Government drawings, specifications, or other data are used for any purpose other than in connection with a definitely related Government procurement operation, the United States Government thereby incurs no responsibility nor any obligation whatsoever; and the fact that the government may have formulated, furnished, or in any way supplied the said drawings, specifications, or other data, is not to be regarded by implication or otherwise as in any manner licensing the holder or any other person or corporation, or conveying any rights or permission to manufacture use, or sell any patented invention that may in any way be related thereto.

This report has been reviewed by the Office of Public Affairs (ASD/PA) and is releasable to the National Technical Information Service (NTIS). At NTIS, it will be available to the general public, including foreign nations.

This technical report has been reviewed and is approved for publication.



GORDON H. GRIFFITH
Project Monitor
Laser & Optical Materials Branch



G. EDWARD KUHL, Chief
Laser & Optical Materials Branch
Electromagnetic Materials Division

FOR THE COMMANDER



MERRILL L. MINGES, Chief
Electromagnetic Materials Division
Materials Laboratory
Air Force Wright Aeronautical Laboratories

"If your address has changed, if you wish to be removed from our mailing list, or if the addressee is no longer employed by your organization please notify AFWAL/MLPO, W-PAFB, OH 45433 to help us maintain a current mailing list".

Copies of this report should not be returned unless return is required by security considerations, contractual obligations, or notice on a specific document.

REPORT DOCUMENTATION PAGE		READ INSTRUCTIONS BEFORE COMPLETING FORM
1. REPORT NUMBER AFWAL-TR-80-4181	2. GOV'T ACCESSION NUMBER <i>A120 720</i>	3. RECIPIENT'S CATALOG NUMBER
4. TITLE (AND SUBTITLE) THALLIUM-DOPED SILICON IR DETECTOR MATERIAL		5. TYPE OF REPORT/PERIOD COVERED Final Technical Report 1 June '79-30 May '80
7. AUTHOR(S) D. E. Schafer		6. PERFORMING ORG. REPORT NUMBER
9. PERFORMING ORGANIZATIONS NAME/ADDRESS Honeywell Inc. Corporate Physical Sciences Center 10701 Lyndale Ave. S., Bloomington, MN 55420		8. CONTRACT OR GRANT NUMBER(S) F33615-79-C-5047
11. CONTROLLING OFFICE NAME/ADDRESS Materials Laboratory Air Force Wright Aeronautical Laboratories Wright-Patterson AFB, OH 45433		10. PROGRAM ELEMENT, PROJECT, TASK AREA & WORK UNIT NUMBERS 61101F, ILIR0110
14. MONITORING AGENCY NAME/ADDRESS (IF DIFFERENT FROM CONT. OFF.)		12. REPORT DATE May 1981
		13. NUMBER OF PAGES 44
		15. SECURITY CLASSIFICATION (OF THIS REPORT) Unclassified
		15a. DECLASSIFICATION DOWNGRADING SCHEDULE
16. DISTRIBUTION STATEMENT (OF THIS REPORT) Approved for public release; distribution unlimited.		
17. DISTRIBUTION STATEMENT (OF THE ABSTRACT ENTERED IN BLOCK 20, IF DIFFERENT FROM REPORT)		
18. SUPPLEMENTARY NOTES		
19. KEY WORDS (CONTINUE ON REVERSE SIDE IF NECESSARY AND IDENTIFY BY BLOCK NUMBER)		
Silicon Thallium	Infrared Detectors Semiconductors	Thermomigration Solution Growth
20. ABSTRACT (CONTINUE ON REVERSE SIDE IF NECESSARY AND IDENTIFY BY BLOCK NUMBER) Thallium-doped silicon crystals were grown by temperature gradient transport from a solution consisting of silicon dissolved in a tin-thallium liquid-metal solvent. Thallium concentrations in excess of 10^{17} cm^{-3} were obtained. The highest thallium doping concentration, $1.33 \times 10^{17} \text{ Tl/cm}^3$, was obtained in material grown using a solvent of 86% Tl and 14% Sn at a growth temperature of 1370°C . Various amounts of shallow acceptor impurities were observed in all of the material grown during the program.		

HD-168 REV 11/74

10 to 16th power

From Hall measurements, boron concentrations as high as $1.9 \times 10^{16} / \text{cm}^3$ were observed. A method for encapsulating thin layers (0.1 ~~mm~~ thick) of 50% Sn and 50% Tl metal solvent within a silicon source-substrate assembly was developed. This approach was found to eliminate the boron contamination and produce uniform crystal growth.

The samples grown exhibited quantum efficiency values as high as 18% at 3.1 microns. The thallium optical cross section at 3.1 microns was $1.45 \times 10^{17} \text{ cm}^{-2}$. Dislocation density measurements were made on some samples which fell in the 5,000 to 8,000/ cm^2 range.

sq. cm

10 to 16th power / sq. cm

FOREWORD

This final report describes work performed by personnel of the Honeywell Corporate Physical Sciences Center, 10701 Lyndale Avenue S., Bloomington, Minnesota, 55420 during the period from 1 June 1979 to 30 May 1980 under Contract F33615-79-C-5047, "Thallium-Doped Silicon Infrared Detector Material." The program was monitored by Capt. James Walcher and Gordon Griffith of the Materials Laboratory, Air Force Wright Aeronautical Laboratories, Wright-Patterson Air Force Base, Ohio.

The program was directed toward establishing feasibility of the gradient-transport solution growth process for growth of silicon heavily doped with thallium for use as an infrared detector material. The author would like to acknowledge the technical assistance of Larry Sheehan and Stewart Dietz in carrying out the crystal growth runs, as well as Brian Anderson, a student aide, who assisted in the development of the wetting step. Robert Hager, Joe Schmit and Walter Scott participated in many stimulating and informative discussions.



Classification For	
GROUP 1	<input checked="checked" type="checkbox"/>
GROUP 2	<input type="checkbox"/>
GROUP 3	<input type="checkbox"/>
GROUP 4	<input type="checkbox"/>
GROUP 5	<input type="checkbox"/>
GROUP 6	<input type="checkbox"/>
GROUP 7	<input type="checkbox"/>
GROUP 8	<input type="checkbox"/>
GROUP 9	<input type="checkbox"/>
GROUP 10	<input type="checkbox"/>
GROUP 11	<input type="checkbox"/>
GROUP 12	<input type="checkbox"/>
GROUP 13	<input type="checkbox"/>
GROUP 14	<input type="checkbox"/>
GROUP 15	<input type="checkbox"/>
GROUP 16	<input type="checkbox"/>
GROUP 17	<input type="checkbox"/>
GROUP 18	<input type="checkbox"/>
GROUP 19	<input type="checkbox"/>
GROUP 20	<input type="checkbox"/>
GROUP 21	<input type="checkbox"/>
GROUP 22	<input type="checkbox"/>
GROUP 23	<input type="checkbox"/>
GROUP 24	<input type="checkbox"/>
GROUP 25	<input type="checkbox"/>
GROUP 26	<input type="checkbox"/>
GROUP 27	<input type="checkbox"/>
GROUP 28	<input type="checkbox"/>
GROUP 29	<input type="checkbox"/>
GROUP 30	<input type="checkbox"/>
GROUP 31	<input type="checkbox"/>
GROUP 32	<input type="checkbox"/>
GROUP 33	<input type="checkbox"/>
GROUP 34	<input type="checkbox"/>
GROUP 35	<input type="checkbox"/>
GROUP 36	<input type="checkbox"/>
GROUP 37	<input type="checkbox"/>
GROUP 38	<input type="checkbox"/>
GROUP 39	<input type="checkbox"/>
GROUP 40	<input type="checkbox"/>
GROUP 41	<input type="checkbox"/>
GROUP 42	<input type="checkbox"/>
GROUP 43	<input type="checkbox"/>
GROUP 44	<input type="checkbox"/>
GROUP 45	<input type="checkbox"/>
GROUP 46	<input type="checkbox"/>
GROUP 47	<input type="checkbox"/>
GROUP 48	<input type="checkbox"/>
GROUP 49	<input type="checkbox"/>
GROUP 50	<input type="checkbox"/>
GROUP 51	<input type="checkbox"/>
GROUP 52	<input type="checkbox"/>
GROUP 53	<input type="checkbox"/>
GROUP 54	<input type="checkbox"/>
GROUP 55	<input type="checkbox"/>
GROUP 56	<input type="checkbox"/>
GROUP 57	<input type="checkbox"/>
GROUP 58	<input type="checkbox"/>
GROUP 59	<input type="checkbox"/>
GROUP 60	<input type="checkbox"/>
GROUP 61	<input type="checkbox"/>
GROUP 62	<input type="checkbox"/>
GROUP 63	<input type="checkbox"/>
GROUP 64	<input type="checkbox"/>
GROUP 65	<input type="checkbox"/>
GROUP 66	<input type="checkbox"/>
GROUP 67	<input type="checkbox"/>
GROUP 68	<input type="checkbox"/>
GROUP 69	<input type="checkbox"/>
GROUP 70	<input type="checkbox"/>
GROUP 71	<input type="checkbox"/>
GROUP 72	<input type="checkbox"/>
GROUP 73	<input type="checkbox"/>
GROUP 74	<input type="checkbox"/>
GROUP 75	<input type="checkbox"/>
GROUP 76	<input type="checkbox"/>
GROUP 77	<input type="checkbox"/>
GROUP 78	<input type="checkbox"/>
GROUP 79	<input type="checkbox"/>
GROUP 80	<input type="checkbox"/>
GROUP 81	<input type="checkbox"/>
GROUP 82	<input type="checkbox"/>
GROUP 83	<input type="checkbox"/>
GROUP 84	<input type="checkbox"/>
GROUP 85	<input type="checkbox"/>
GROUP 86	<input type="checkbox"/>
GROUP 87	<input type="checkbox"/>
GROUP 88	<input type="checkbox"/>
GROUP 89	<input type="checkbox"/>
GROUP 90	<input type="checkbox"/>
GROUP 91	<input type="checkbox"/>
GROUP 92	<input type="checkbox"/>
GROUP 93	<input type="checkbox"/>
GROUP 94	<input type="checkbox"/>
GROUP 95	<input type="checkbox"/>
GROUP 96	<input type="checkbox"/>
GROUP 97	<input type="checkbox"/>
GROUP 98	<input type="checkbox"/>
GROUP 99	<input type="checkbox"/>
GROUP 100	<input type="checkbox"/>

A

TABLE OF CONTENTS

	<u>Page</u>
SECTION I INTRODUCTION.	1
SECTION II EXPERIMENTAL PROCEDURES	7
Gradient Transport Solution Growth.	7
Wetting Step.	14
Hall Measurements	17
Optical Measurements.	19
SECTION III RESULTS AND DISCUSSION.	21
Tl Doping	21
Quantum Efficiency.	27
Shallow Impurities.	29
Crystal Morphology.	37
SECTION IV CONCLUSIONS AND RECOMMENDATIONS	42
References.	44

LIST OF ILLUSTRATIONS

<u>Figure</u>		<u>Page</u>
1	Relationship Between Compositions and Temperatures Occurring at Various Stages of Solution Growth Process.	7
2	Solubility of Silicon in Tin and Thallium Solvents .	9
3	Configurations of Starting Materials and Ampoule Used in Solution Growth Runs	12
4	Heating Apparatus for Wetting Step	16
5	Configurations of Materials for Wetting Step	17
6	Thallium Doping Concentrations Observed in Growth Runs During the Program.	22
7	Estimated Values of the Distribution Coefficient for Thallium from Tin-Thallium-Silicon Solutions . .	26
8	Photoionization Absorption Observed in Sample CS-6 .	29
9	Carrier Concentration Versus Temperature in Sample CS-5	30
10	Carrier Concentration Versus Temperature in Sample CS-13.	32
11	Optical Absorption Spectrum of Sample CS-8 in Region of Several Impurity Absorption Lines	33
12	Growth Morphology Observed at Beginning of Program .	38
13	Growth Morphology Obtained at End of Program	40

LIST OF TABLES

<u>Tables</u>		<u>Page</u>
I	Summary of Wetting Tests	18
II	Optical Conversion Factors for Impurities in Silicon at 8K.	20
III	Summary of Impurity Analysis	23
IV	Summary of Quantum Efficiency Measurements	28
V	Dislocation Densities in Solution-Grown Si(Tl).	41

SECTION I

INTRODUCTION

In order to carry out infrared imaging more efficiently than is possible with current systems, the so-called "second-generation" concept of an infrared detector array integrated with silicon electronics for signal readout (and perhaps signal processing as well) is being developed. Realization of this concept requires development of an optimized detector material, a means for fabricating uniform arrays of detectors from this material, and integration of these arrays with silicon electronics.

One approach for carrying out this concept is to develop suitably doped silicon as the detector material and thereby take advantage of the relative ease with which processing steps such as ohmic contact formation and metallizations can be performed on silicon. This processing advantage has not proved to be great enough to provide a solution to the most challenging approach to silicon detector/electronics integration pursued in the past (i.e. a monolithic approach), but has still made it possible to pursue some other approaches to integration in a straightforward way. For example, the use of bump interconnection technology to connect separately prepared chips of detector material and electronics has resulted in focal planes which represent the state of the art insofar as image quality.

Mercury cadmium telluride, (Hg,Cd)Te, has been used in infrared imaging systems for several years in the form of small arrays of individually wired detectors. This material is now also being developed for use in second-generation integrated focal plane arrays. The challenging part of this approach is in developing

the understanding of defect chemistry and processing steps in this material to the point where uniform arrays of photovoltaic detectors can be fabricated reproducibly and integrated with silicon electronics.

Of the two materials, (Hg,Cd)Te is presently receiving the greater amount of attention for focal plane applications because of its higher operating temperature in comparison to extrinsic detectors and more efficient absorption of infrared radiation. However, it is not clear that the development of the technology for integration of (Hg,Cd)Te with silicon electronics will be able to keep pace with demands for focal planes of increasing size and complexity. For this reason, the development of silicon detector material for various wavelength ranges remains potentially important in the overall advancement of focal plane technology.

The major challenge in pursuing the extrinsic silicon approach is the achievement of proper doping of the detector material. This has not always been straightforward. The main impurity used should preferably have an ionization energy equal to the energy of the longest wavelength radiation to be detected. The material must be doped with this impurity as heavily as is needed to give efficient absorption of the radiation to be detected, but without doping nonuniformities which cause detector nonuniformities when the material is made into a detector array. Such nonuniformities have been a problem at times in arrays made from Czochralski or float-zone material. Also, the material must be made free of shallower electronically active levels or crystalline defects which might limit the responsivity or operating temperature of the detectors. An example of an unexpected occurrence of such a defect is the In-X acceptor level found in indium-doped silicon, which lowered the operating temperature of Si(In) detectors until the defect was identified as an indium-carbon complex and carbon incorporation suppressed during growth.

The acceptor thallium has been identified as a promising dopant in silicon for detection of infrared radiation in the 3 to 5-micron atmospheric window. The ionization energy of this acceptor is 0.246 eV^1 which corresponds to a cutoff wavelength of 5.04 microns and makes it responsive to radiation in the entire 3 to 5 micron range. The binding of holes to thallium acceptors appears to fall in the same theoretical framework as that for the other group IIIA acceptors (hydrogenic effective-mass theory) so that processes relevant to photoconductive detector operation -- photoionization, thermal generation and recombination -- can be understood within an established theoretical framework. In addition, the diffusion coefficient of thallium in silicon is low², so that precipitation of this dopant is not expected to be a problem. However, other properties of thallium in silicon present difficulties in the crystal growth of detector-grade material. The major factor is the low miscibility of thallium with either solid or liquid silicon. The immiscibility in molten Si interferes with the stability of Czochralski or float-zone growth of Si(Tl). Attempts to grow thallium-doped silicon by these techniques have yielded material that is either too lightly doped or polycrystalline. The highest thallium doping achieved in float-zone growth³ has been $2 \times 10^{15} \text{ cm}^{-3}$. Based on some of the information presented below, this would correspond to a quantum efficiency of 0.3 percent at 3.1 microns, which is unacceptably low. Silicon much more heavily doped with thallium (up to about $2 \times 10^{17} \text{ cm}^{-3}$) has been produced in some simple experiments⁴ involving quenching of liquid Si-Tl mixtures from temperatures above 1400°C , but the resulting material has been polycrystalline. Clearly an alternative growth technique is needed to produce single crystals of heavily doped material. Another factor in designing a growth procedure is the high vapor pressure of thallium (approaching one atmosphere at the silicon melting point). This requires the use

hot-walled closed container for the growth process in order to prevent condensation of thallium away from the growth region.

The thrust of this program has been to investigate the feasibility of an alternative crystal growth process, gradient transport solution growth, for producing detector-grade thallium-doped silicon. The central issues of this investigation have been whether the growth process is feasible for producing crystals of the desired morphology and whether the thallium concentration can be increased to the point where photoionization absorption by thallium acceptors becomes high enough for efficient infrared detection.

Specific objectives of the project have been to:

Demonstrate the growth of single crystals of thallium-doped silicon 1" in diameter

Achieve thallium concentrations of $10^{17}/\text{cm}^3$ or greater

Assess the potential of the growth process for satisfying other detector-related material requirements such as purity, crystalline perfection, and doping uniformity.

In respect to the thallium doping issue, progress has been relatively straightforward. As discussed below, it has been possible to carry out the gradient transport solution growth process using fairly thallium-rich solvents and thereby to obtain material doped fairly closely to the thallium solubility limit. However, control of the growth morphology has developed slowly, and has involved making substantial changes in both the configuration of the materials used in the growth process and the methods for setting up the crystal growth runs. Single crystals of good morphology were demonstrated after the solution

layer used in the growth process was reduced substantially in thickness, although the capillary wetting step used to set up this thin solution layer could not be carried out for the thallium-rich solutions which would give the highest thallium doping. To summarize, the growth procedure has been developed to the point where high thallium doping or good crystal morphology (but not both simultaneously) could be obtained.

The specific results of the program have been:

- Growth of single-domain crystals up to 20mm in diameter
- Achievement of a maximum Tl doping of $1.33 \times 10^{17} \text{ cm}^{-3}$
- Observation of quantum efficiencies up to 18 percent as projected for a 1-mm detector thickness
- Observation of residual impurity contamination by boron and perhaps aluminum at about the 10^{16} cm^{-3} and 10^{15} cm^{-3} levels, respectively; the boron contamination has been eliminated through the use of an encapsulated solution for the growth, but the aluminum contamination has persisted
- Observation of dislocation densities of several thousand per cm^2 .

These results constitute initial confirmation that the gradient transport solution growth process is capable of producing material adequately doped for use in detectors. However, the detector performance of solution-grown Si(Tl) remains uncharacterized because the high level of shallow impurities observed in the crystals eliminated the possibility of responsivity measurements at the operating temperatures of interest.

It seems likely that the solution growth process can be developed to the point where crystals having both good morphology and high thallium doping can be grown whose purity is at least adequate for carrying out detector performance measurements. The issues to be addressed at that point are whether material properties which cannot be as easily controlled within the context of this growth process (such as the dislocation density and the presence of incorporated tin) are compatible with optimized detector operation.

SECTION II EXPERIMENTAL PROCEDURES

GRADIENT TRANSPORT SOLUTION GROWTH

In this program silicon crystals were grown from a solution consisting of silicon dissolved in a molten mixture of the metals thallium and tin. (The molten metal mixture is referred to as the solvent for the growth process.) The principles of the growth method are illustrated in Figure 1 using a binary phase diagram in which the two components of the system are silicon and tin-thallium metal (the possibility of inhomogeneity in the tin/thallium ratio of the metal during growth is ignored for

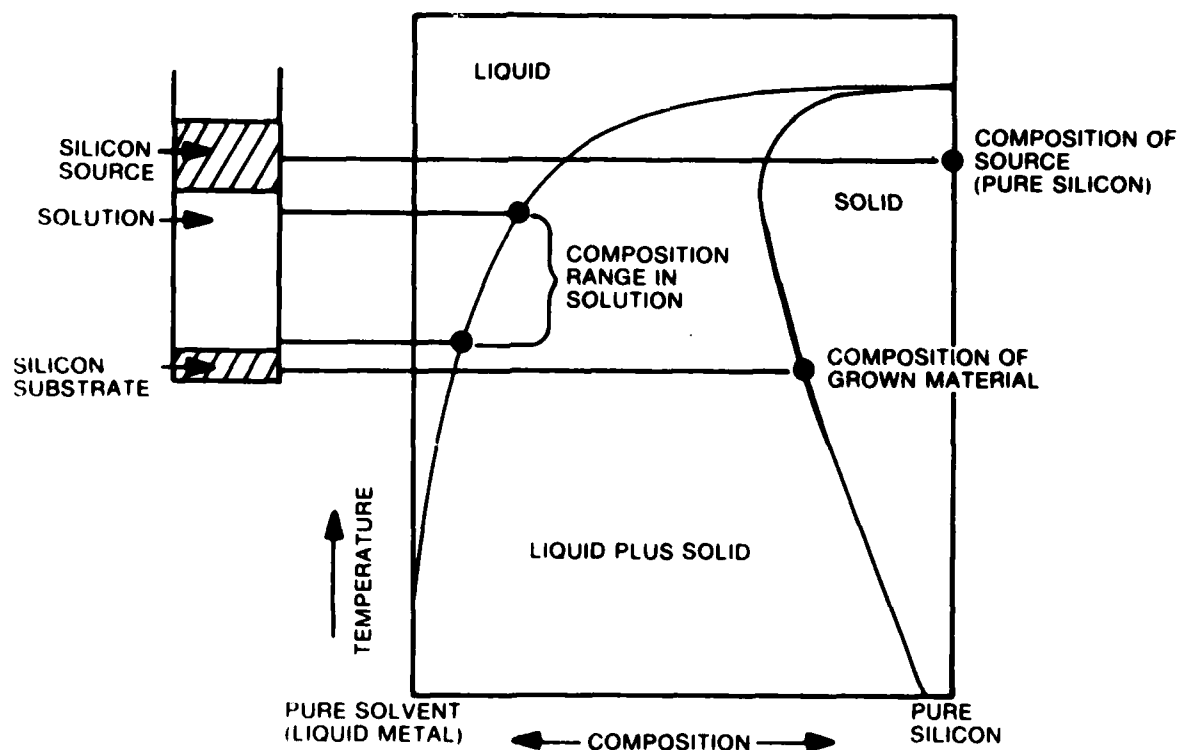


Figure 1. Relationship Between Compositions and Temperatures Occurring at Various Stages of Solution Growth Process

purpose of this illustration). Also shown in the figure is the physical arrangement of the materials involved in the growth process. A silicon substrate is covered with the liquid metal, which in turn is covered with silicon source material. As indicated by the liquidus of the phase diagram, the metal has the capacity to dissolve appreciable amounts of silicon at high temperature; this solubility increases steadily with increasing temperature.

The growth process begins when, after initial heating of the materials near the desired growth temperature (and the associated degree of dissolution of silicon from the source and substrate), a temperature gradient is introduced such that the source is made hotter than the substrate. Again because of the slope of the metal-silicon liquidus, the solution tends to become richer in dissolved silicon near the (hotter) source as compared to a lesser concentration of dissolved silicon near the (cooler) substrate. The temperatures and silicon-metal compositions of the solution at these two positions are marked on the phase diagram. The difference in silicon content at the top and the bottom of the solution represents a silicon concentration gradient, and diffusion of silicon in the solution causes a net transport of silicon toward the substrate. As a result, the solution tends to become supersaturated with silicon at the substrate and recrystallizes silicon there. The recrystallized silicon incorporates metal from the solution as well, according to the solid solubility of the metal in silicon at the substrate temperature, which is represented by the solidus curve of the phase diagram.

The net effect of the process is that the solution layer migrates upward through the source wafer, and leaves a trail of doped silicon behind itself. This is expected to continue as long as the temperature gradient is maintained and source silicon is

present.

The phase equilibria and the details of the solution growth process in the ternary silicon-tin-thallium system are undoubtedly more complicated than the binary representation used in Figure 1, although it is expected that transport of silicon can still occur in the same way and lead to deposition of silicon. The complicating factors are first that the system is a ternary one so that the tin/thallium ratio may in principle vary from point to point in the solution, most likely from top to bottom. Secondly, and more fundamentally, the mixing of thallium and silicon versus

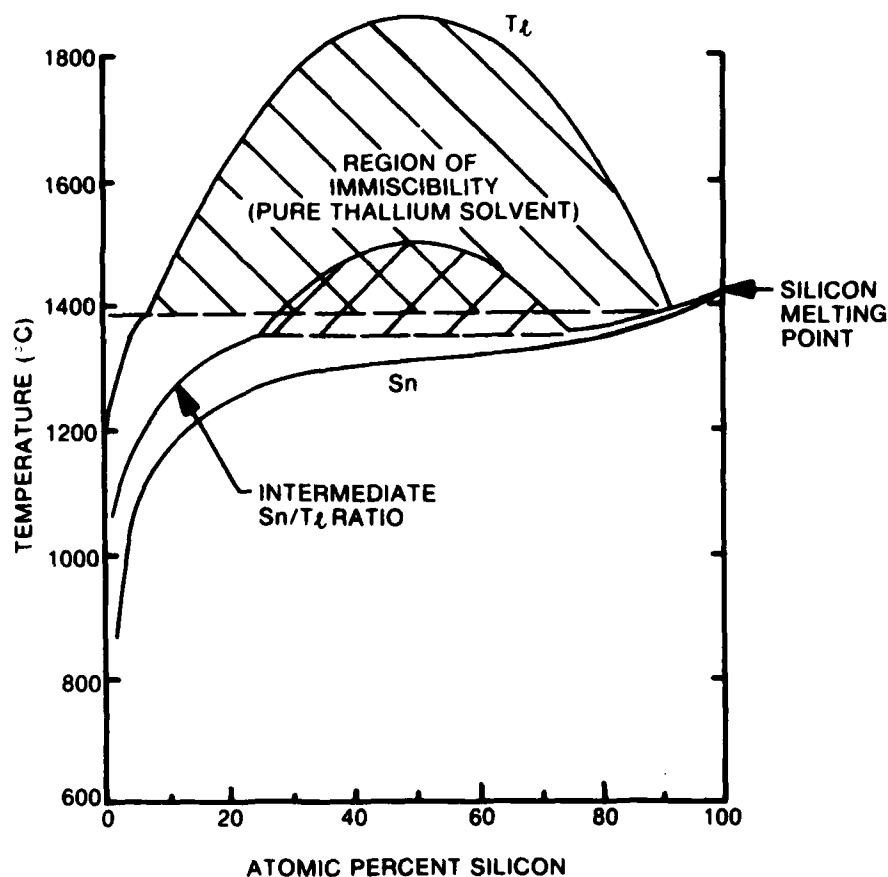


Figure 2. Solubility of Silicon in Tin and Thallium Solvents

temperature does not follow the kind of phase diagram used in Figure 1, but rather exhibits a substantial miscibility gap. Available phase diagram information on the binary systems Si-Sn⁵ and Si-Tl⁶ is shown in Figure 2, as well as a third, more speculative curve illustrating the possible features of silicon versus solution coexistence for an intermediate Sn-Tl composition.

The Si-Sn liquidus is of the type shown in Figure 1, so that the description of solution growth given above would hold exactly if a pure Sn solvent were used for the growth process. In the Si-Tl system, however, the liquidus is markedly different, in two respects. First, the silicon concentration at the liquidus is much lower than in the Si-Sn system for most temperatures of interest (1386°C and below). This means that silicon is much less soluble in liquid thallium than in liquid tin and that the capacity for silicon transport is relatively low in a pure thallium solvent. The second important aspect of the Si-Tl liquidus is that it is interrupted by a miscibility gap, a range of compositions and temperatures in which the silicon thallium liquid mixture is unstable with respect to separation into a Tl-rich liquid and a Si-rich liquid. The Si-Tl liquidus shown in Figure 2 is based on a model and parameter values given by Thurmond and Kowalchik⁷. The sequence of Tl-Si liquid mixtures which coexist with solid silicon as the temperature is raised (i.e. the liquidus) jumps discontinuously from Tl-rich to Si-rich as the temperature is raised past one particular value. Thurmond and Kowalchik give an estimate of 1386°C as the temperature of the discontinuity, not far below the silicon melting point. These authors also predict quite a wide miscibility gap, with less than 10 atomic percent silicon on the Tl-rich side and over 90 atomic percent silicon on the other.

As one moves away from a pure thallium solvent by adding tin, the discontinuity in the liquidus is expected to diminish in size and move to lower temperatures until above a certain tin content, the miscibility gap is expected to disappear altogether. As the tin content is increased, the capacity for silicon transport (and thus the achievable growth rates) is expected to increase, but the thallium doping is expected to decrease because the thallium becomes less concentrated in the growth solution.

The occurrence of immiscibility in the solution would undoubtedly complicate the situation, but it is not clear whether the growth process would be disrupted or not. If the solution were to separate, the Tl-rich liquid would settle to the bottom because of its greater density and the Si-rich liquid would rise to the top, thus maintaining the monotonic increase in silicon concentration from bottom to top and not incompatible with a net downward transport of silicon.

Two slightly different configurations of source, substrate and solution were used during the program. The first is shown in Figure 3a. This arrangement was used in early growth runs to investigate the thallium doping level achievable by solution growth. In this arrangement a 4-mm deep well was milled out of the substrate. The source material was ground down to a diameter which fit into the substrate well. A lip on the source rested on the wall of the substrate well so that a source-to-substrate gap of about 1mm was maintained in the region occupied by the tin-thallium solvent. For growth runs in this configuration, the tin-thallium alloy was pressed into a disc of thickness 1mm and laid into the substrate well in solid form during the room-temperature loading procedure. The volume of tin-thallium alloy used was typically 0.85 to 0.90 percent of the available interior volume of the assembly to avoid spillage of the solution.

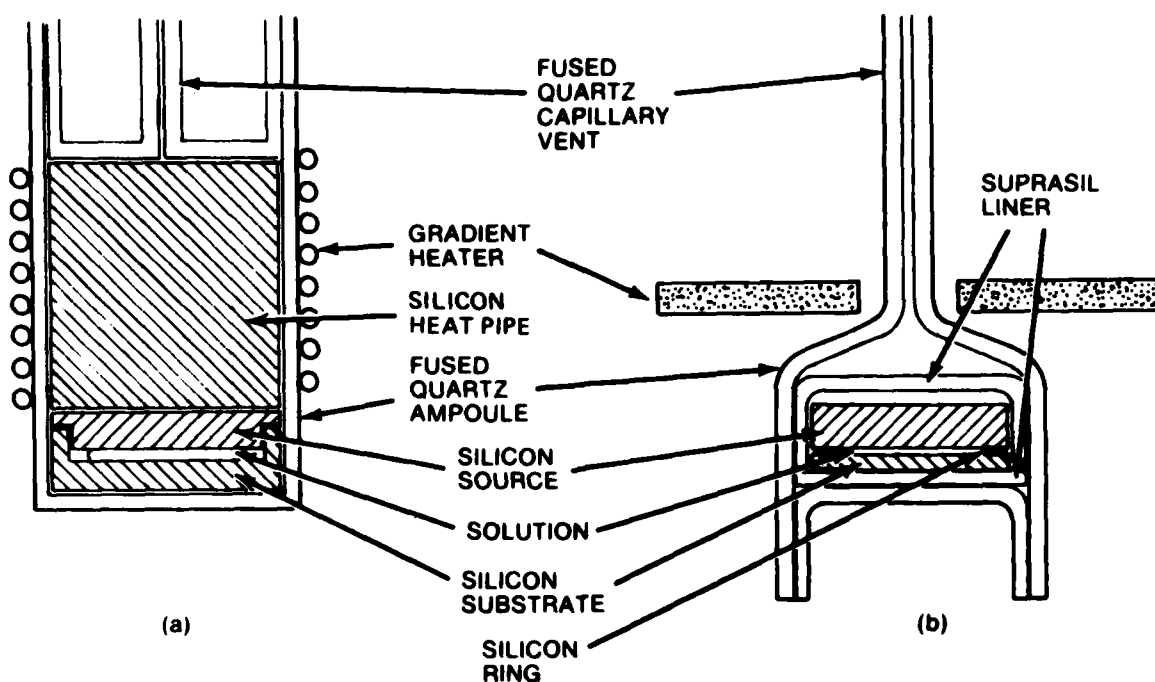


Figure 3. Configurations of Starting Materials and Ampoule Used in Solution Growth Runs

These starting materials were loaded into a flat-bottomed quartz ampoule as shown in Figure 3a. A relatively large cylinder of silicon was then added on top of these pieces to act as a heat pipe and aid in setting up the required temperature gradient. A capillary restriction was fused into the ampoule at the location shown to retard thallium evaporation out of the ampoule. A few turns of Kanthal wire were wound around the ampoule at the location of the heat pipe. The entire ampoule was then loaded into the growth furnace (a 3-zone Thermco "Mini-Brute" furnace stood vertically) and evacuated and backfilled with argon several times to purge it of oxygen before heating. The open end of the ampoule was connected into a tee fitting which passed argon over the ampoule end thus maintaining inert ambient conditions there while allowing the ampoule to remain near ambient pressure.

Downstream from the ampoule, the argon was passed through a trap to prevent thallium vapor from escaping the system.

The crystal growth furnace was set for a flat temperature profile and raised to a temperature near the desired growth temperature. The heater wound on the ampoule was run at about 100 watts to produce a temperature gradient of $10^{\circ}\text{C}/\text{cm}$ in the vicinity of the growth assembly (as determined in a separate profiling measurement). Finally, the main furnace set point was adjusted until the exact desired growth temperature was projected at the growth assembly.

The second configuration, shown in Figure 3b, was adopted after the stability and morphology of the growth process in configuration 3a proved to be inadequate for further use. In this configuration, a smaller source-to-substrate gap (of the order of 0.1mm) was used. The source and substrate were each flat, and the gap between the two pieces was maintained by a 0.1mm-thick silicon ring which also served as a side wall defining the lateral extent of the solution.

A major emphasis in using the configuration of Figure 3b was to fill the source-substrate gap more fully with the tin-thallium solvent and to establish oxide-free interfaces between the solution and the silicon pieces prior to the growth run. This emphasis resulted from voids and poor growth morphology observed in early growth runs using configuration 3a. In order to achieve these conditions, a preliminary heating step was developed as described on the following page.

At about the same point in the program, changes were made in the design of the ampoule and gradient heater used in the growth runs. The ampoule retained the same function as before, but was made more compact and easier to load. The new gradient heater was a flat-plate resistive element made of carbon, mounted horizontally over the ampoule bulb and housed in an argon-filled shroud. The use of carbon enabled the gradient heater to operate at significantly higher temperatures (over 1400°C) than the Kanthal wire used previously.

WETTING STEP

As mentioned above, a preliminary heating step was carried out to promote more complete and void-free filling of the source-substrate gap with tin-thallium metal and establishment of oxide-free interfaces between the metal and the silicon pieces. Such conditions were considered desirable from the standpoint of improving the stability and uniformity of the growth process. The most reliable approach to covering the silicon pieces with the metal was thought to be to promote capillary action or a tendency of the metal to wet the silicon surfaces. In general, it was found that only by heating the materials to fairly high temperatures (over 1200°C) under oxygen and water vapor partial pressures of 10^{-2} torr or less could such wetting action occur. At lower temperatures, the contact angle between the liquid metal and a silicon surface was always observed to be greater than 90 degrees that is, non-wetting. At higher oxygen partial pressures (associated with inadequately pure argon or poor vacuum) the tin-thallium metal dissolved away silicon at existing points of contact without flowing over the remainder of the silicon surfaces. However, once tin-thallium metal had been

caused to wet a silicon surface at high temperature it had a tendency to continue coating the silicon upon further temperature cycling. In general, this enabled the assembly to be inspected at room temperature following the wetting step, followed in turn by the crystal growth run.

The apparatus used for heating the materials is shown in Figure 4. It consisted of a horizontal quartz tube which was either pumped out through a liquid nitrogen cold trap or flushed with argon at atmospheric pressure. Two 300-watt tungsten lamps, focused on the silicon source and substrate from above and below, were used for rapid heating. Judging from the yellow-orange glow given off by the assembly when the lamps were turned off, the assembly typically reached temperatures of 1100° - 1200° C. The duration of the heating process was kept to five minutes or less because of rapid condensation of metal vapors on the relatively cool walls of the quartz tube. Following the wetting step the assembly was unloaded from the tube and the degree of filling of the source-substrate gap with tin-thallium metal was determined by X-ray radiography. This method consisted of placing the sample between a point-like X-ray source (1mm^2 aperture at a distance of about 1 meter from the sample) and a photographic plate. Silicon has a sufficiently low X-ray absorption coefficient that radiation passing through a sample several millimeters thick exposes the plate in a reasonable amount of time. The tin-thallium metal is relatively opaque, however, and produces shadows on the plate which appear as light areas when the film is developed. Voids in the metal layer show up as darker areas in the region where metal is desired.

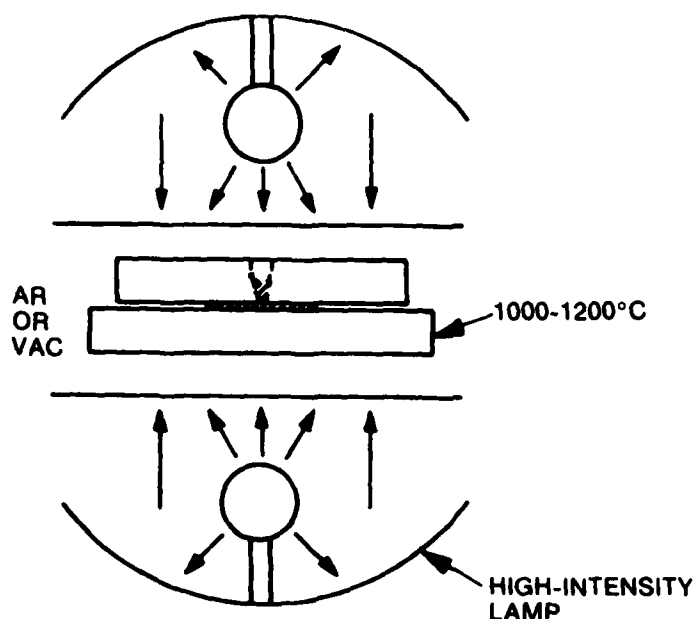


Figure 4. Heating Apparatus for Wetting Step

Several starting configurations of the silicon and metal were used in approximately 30 tests; three of the configurations tried are illustrated in Figure 5. The relative successes of the different arrangements are summarized in Table I. The most successful arrangement was 51) when carried out under a vacuum of 10^{-2} torr or less. In this approach, a funnel-shaped hole was sand-blasted through the silicon source. A pellet of Sn-Tl metal placed in the funnel would typically remain stationary upon initial melting at 200° - 300° C but then would flow down through the hole at higher temperatures. Once the metal encountered the source-substrate gap it would usually be drawn into the gap by capillary action. The advance of the liquid metal meniscus was not always regular, however, and void (non-wetted) areas of 5 percent - 50 percent of the source-substrate gap region were observed by X-ray radiography following the heating step. Two of the cases in which the void area was exceptionally low (around 5 percent) were used for growth runs CS-12 and CS-13. The hole in

the source was filled with a silicon plug prior to the growth run.

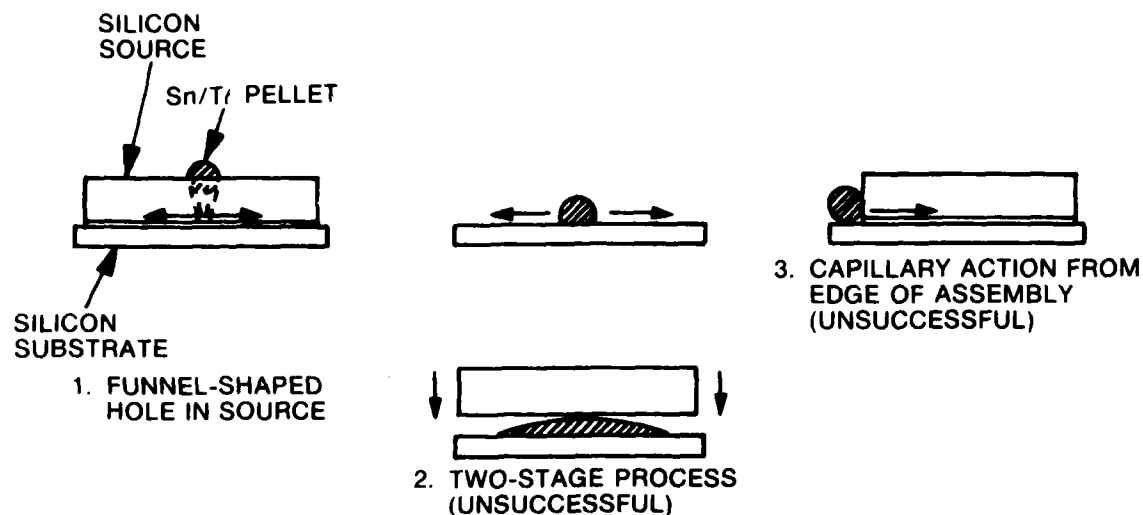


Figure 5. Configurations of Materials for Wetting Step

HALL MEASUREMENTS

Following crystal growth runs, Hall and resistivity measurements were made on slices taken from growth assemblies. The measurements were carried out in a dc mode at 8KG. The system used for these measurements includes a Janis Model 8DT research dewar which can be cooled to liquid helium temperatures. The sample temperature was controlled to 0.1°K with a Lakeshore Cryotronics DT-500 temperature controller. The system can measure samples in the van der Pauw configuration up to a resistance of 10^9 ohms and bridge-type samples up to 10^{13} ohms.

The Hall data discussed below were used to obtain carrier concentration values versus temperature using the relation $p = r/eR_H$. The Hall scattering factor, r , was always taken as unity.

TABLE I. SUMMARY OF WETTING TESTS

Test Nos.	Metal Composition	Configuration	Dates	No. of Potential Growth Assemblies	Void Area (%)
1-3	$\text{Sn}_{0.5}\text{Ti}_{0.5}$	Funnel-shaped hole (1) centered in source	8/29-9/6	2 (one used for growth CS-10)	5
6, 7, 12, 13	$\text{Sn}_{0.5}\text{Ti}_{0.5}$	Open-faced (2) (two-step process)	9/8-10/1	2	10-50
8, 9	$\text{Sn}_{0.5}\text{Ti}_{0.5}$	Metal drawn from edge of Si pieces (3)	9/13, 9/14	0	
10, 14-18	$\text{Sn}_{0.5}\text{Ti}_{0.5}$	Off-center funnel-shaped hole in source (1)	9/17-10/29	4 (1 with 5% void used for growth CS-11)	15-30
19-23	$\text{Sn}_{0.5}\text{Ti}_{0.5}$	Off-center funnel; mesas etched in substrate (1)	10/24-11/20	0	
24, 25, 30, 31	$\text{Sn}_{0.5}\text{Ti}_{0.5}$	Off-center funnel; spacer ring (1)	11/28-12/20	4	20-50
26-29	$\text{Sn}_{0.25}\text{Ti}_{0.75}$	Off-center funnel; spacer ring (1)	12/12-12/17	0	

There is undoubtedly some error associated with this, since analyses of Hall measurements on indium-doped silicon have indicated that the r factor may deviate from unity by as much as a factor of two, especially above room temperature. However, there is no well-defined way to transfer these results quantitatively to the present case. The values of impurity concentration obtained through the use of $r = 1$ were therefore regarded as relative values, useful for determining progress in the thallium doping and purity of the material, but subject to errors in absolute magnitude of up to a factor of two. The concentrations of various acceptors in the material were inferred through the use of a least-squares fitting program which could be set up to use from one to six acceptor levels in fitting the data. Each of three parameters describing each acceptor level used (ionization energy, degeneracy, or concentration) could be specified as variable or fixed at a given value.

OPTICAL MEASUREMENTS

Information on the impurity content of some of the crystals was obtained via optical absorption measurements. Samples were lapped and polished with about a one-half degree taper to eliminate the appearance of interference fringes in the transmittance versus wavelength and were cooled to 8K for transmittance measurements. The transmittance (T) was measured using a Digilab FTS-14 spectrometer at a resolution of 2cm^{-1} and converted to absorption coefficient (α) using the relationship

$$T = \frac{(1-R)^2 \exp(-\alpha d)}{1-R^2 \exp(-2\alpha d)}.$$

The reflectivity (R) was set at 0.3. To measure impurity absorption accurately in some spectral regions, the intrinsic silicon lattice absorption was subtracted off. The reference absorption spectrum subtracted away was that of a high-purity vacuum float-zoned crystal. The impurity contents of the crystals were determined from the intensities of absorption lines known to be associated with impurities in silicon. The conversion factors for these determinations are listed in Table II for several impurities. The calibration of the thallium absorption line at 1907cm^{-1} was obtained from Hall and optical measurements on sample CS-6.

TABLE II. OPTICAL CONVERSION FACTORS FOR
IMPURITIES IN SILICON AT 8K

Impurity	Line Position (cm^{-1})	Concentration (cm^{-3})
Boron	666	$[B] = \text{line area} \times 1.48 \times 10^{14}$
Boron	continuum near 700cm^{-1}	$[B] = \alpha \times 1.83 \times 10^{15}$
Aluminum	472	$[Al] = \text{line area} \times 4.2 \times 10^{13}$
Gallium	510	$[Ga] = \text{line area} \times 5 \times 10^{13}$
Indium	1175	$[In] = \text{line area} \times 2 \times 10^{15}$
Thallium	1907	$[Tl] = \text{line area} \times 1 \times 10^{16}$
		Note: line area is absorption coefficient in cm^{-1} inte- grated over frequency in cm^{-1} .

SECTION III

RESULTS AND DISCUSSION

Tl DOPING

As discussed in Section I, a major objective of the program was to achieve thallium doping at or above 10^{17} cm^{-3} in silicon grown by gradient transport from tin-thallium solutions. Since the growth process was believed to involve near-equilibrium coexistence between the solution and the material grown from it, the thallium doping of the grown material was expected to depend mainly on the growth temperature and the tin/thallium ratio of the metal solvent. In the investigation of the thallium doping, therefore, several growth runs were carried out using various ratios of tin to thallium in the solution and various growth temperatures. The thallium acceptor content of the grown material was measured by the Hall and/or optical absorption techniques described above.

The results of several runs are plotted in Figure 6 and listed in Table III. In general, as either the thallium/tin ratio or the temperature was increased the thallium doping concentration was found to increase. The highest thallium doping concentration, $1.33 \times 10^{17} \text{ Tl/cm}^3$, was obtained in material grown using a solvent of 86 percent Tl and 14 percent Sn at a growth temperature of 1370°C . This represents a significant advance in our ability to satisfy material requirements for infrared detectors.

A simple model was developed to account for the thallium doping and to allow extrapolation to other growth temperatures and solvent compositions. The basic hypothesis was that the thallium doping could be given by the product of the thallium concentration in the solution and a distribution coefficient for thallium which depended only on temperature:

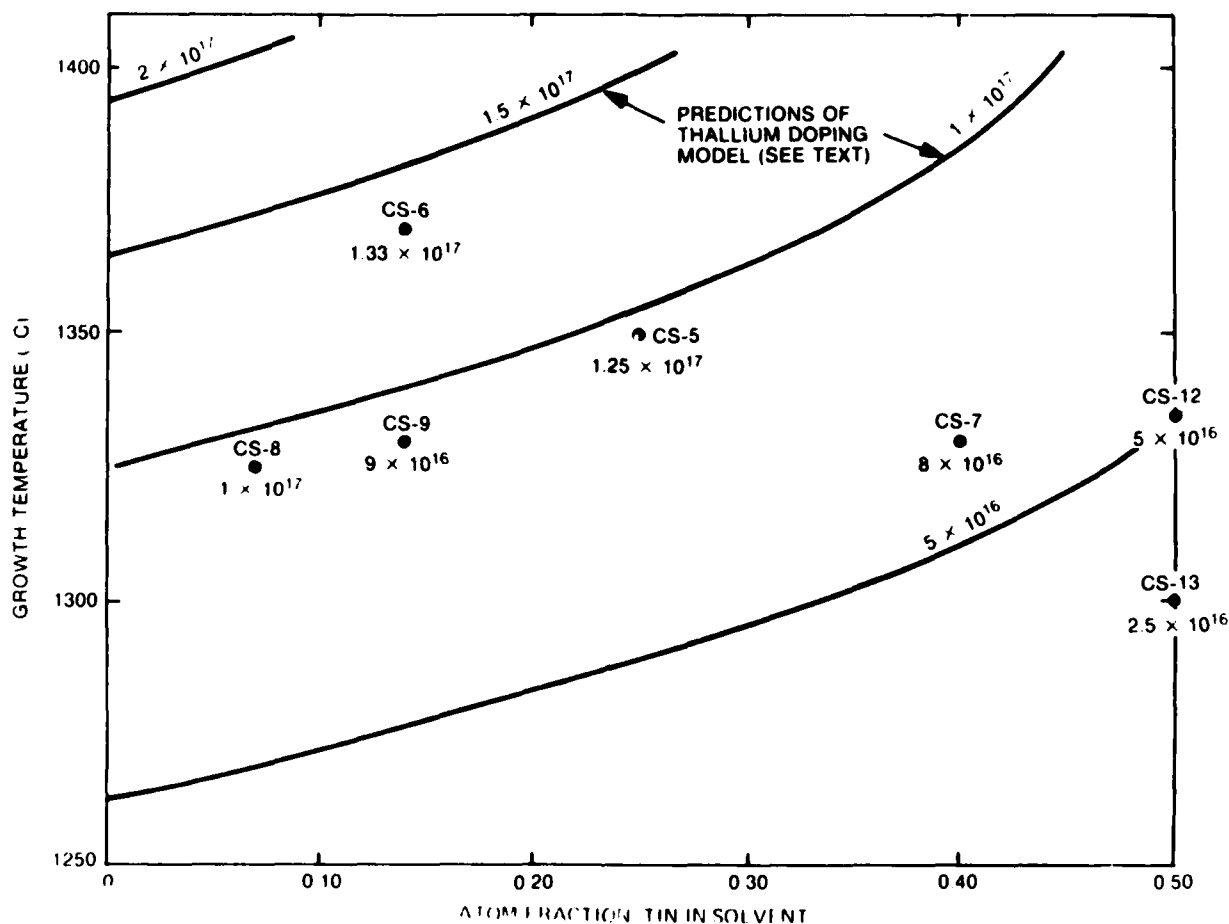


Figure 6. Thallium Doping Concentrations Observed in Growth Runs During the Program

$$[Tl]_{\text{SOLID}} = k_{Tl}(T) [Tl]_{\text{LIQUID}}$$

This approach is undoubtedly oversimplified since the affinity of the solution for thallium (and therefore the distribution coefficient) is expected to be influenced by its tin content as well as the temperature. Accordingly, little significance was attached to the exact values of $k(T)$ which best fit the data, aside from their overall magnitude (low to mid- 10^{-6} over 1300° - 1400°C). The extrapolation of the best-fitting functional form is considered

TABLE III. SUMMARY OF IMPURITY ANALYSIS

Sample No.	Solvent Composition	Growth Temperature	Hall Analysis			Optical Analysis	
			Ti	Shallow Acceptors	Compensation	Ti	Shallow Acceptors
CS-4	Ti _{0.75} Sn _{0.25}	1325	No Growth				
CS-5	Ti _{0.75} Sn _{0.25}	1350	1.25×10^{17}	1.65×10^{16} at 0.048eV	1.6×10^{15}		
CS-6	Ti _{0.86} Sn _{0.14}	1370	$1.33 \times 10^{17}(1)$	2×10^{15} at 0.075eV	7×10^{13}		$<10^{14}$ B, 5×10^{14} A;
CS-7	Ti _{0.60} Sn _{0.40}	1330	1.3×10^{17}	1.2×10^{16} at 0.049eV	1.1×10^{15}	8×10^{16} T;	$<5 \times 10^{14}$ A, 3×10^{15} B
CS-8	Ti _{0.93} Sn _{0.07}	1325				1.0×10^{17} T;	8×10^{15} B, 3×10^{14} A;
CS-9	Ti _{0.86} Sn _{0.14}	1330				9×10^{16} T;	1.5×10^{16} B, $<2 \times 10^{14}$ A;
CS-10	Ti _{0.5} Sn _{0.5}	1330	No Growth				
CS-11	Ti _{0.5} Sn _{0.5}	1310	No Growth				
CS-12	Ti _{0.5} Sn _{0.5}	1300	$3.7 \times 10^{15}(2)$	2.2×10^{15} at 0.067eV	0 ± 10^{13}		
CS-13	Ti _{0.5} Sn _{0.5}	1335	2.5×10^{16}	3.4×10^{15} at 0.065eV	2.6×10^{15}		

(1) Used to calibrate the intensity of the $1907\text{cm}^{-1}\text{Tl}$ line.

(2) Thallium concentration very uncertain; no Hall data taken above 300K.

valid only for fairly thallium-rich solvents, ranging up to 40 percent tin content, and for temperatures between 1300C and 1400°C.

The determination of effective values of $k(T)$ from the results of individual growth runs required estimation of the thallium concentration in the growth solutions used. This was carried out using regular solution theory as applied to silicon-dopant binary systems by Thurmond and Kowalchik.⁷ Since the tin/thallium ratio is known, the only unknown quantity involved in determining the thallium concentration in the solution is the atom fraction of dissolved silicon, x_{Si} , the expression used to estimate this was:

$$\ln x_{Si} = \frac{H^f}{R} \left(\frac{1}{T_m} - \frac{1}{T} \right) - (1-x_{Si})^2 \left[y \frac{(a_1 - b_1 T)}{RT} + (1-y) \frac{(a_2 - b_2 T)}{RT} \right] \quad (1)$$

where y is the atom fraction of tin in the solvent (i.e. the solvent composition is $Sn_y Tl_{1-y}$) and

H^f (silicon heat of fusion) = 12,100 cal/mole

R (gas constant) = 1.987 cal/mole-deg

T_m (silicon melting point) = 1410°C

a_1 = 8145 cal/mole

b_1 = 1.50 cal/mole-deg

a_2 = 16,600 cal/mole

b_2 = 3.8 cal/mole-deg

The a's and b's are parameters used by Thurmond and Kowalchik to represent the contributions to excess free energy of mixing in the liquid phase due to interactions between unlike atoms. Here the subscript 1 denotes Si-Sn interactions and 2 denotes Si-Tl interactions. Available thermochemical data indicate that interactions between Sn and Tl (which would introduce another term in the square bracket in Eq. 1) are relatively small and can be neglected.⁸

The magnitudes of $\ln k(T)$ obtained for the growth runs using the thallium-rich solvents are plotted versus $1/T$ in Figure 7. The values can be roughly fit by a function of the form $\ln k(T) = A - B/T$ which is characteristic of the distribution coefficients of dopants in silicon.⁹ The values used to fit the data were

$$\ln k_{Tl}(T) = 67.7 = \frac{2.76 \times 10^4 K}{T}$$

This chosen function $k(T)$ was then used in conjunction with Eq. (1) to generate estimated thallium doping values over the range 1250° - 1400°C and 0.0-0.4 Sn fraction in the solvent. The results are plotted in Figure 6 as contours of constant Tl doping.

Two comments can be made about the results. The first is that on the whole, the thallium doping achieved in this range of growth conditions appears to be more sensitive to the growth temperature than to the amount of tin present in the solvent. The reason for this is that thallium is the major component of the solution over this entire range of growth conditions ranging from 0.5 to 0.9 in atom fraction. The other major aspect of the results is that a maximum thallium concentration of about $2 \times 10^{17} \text{ cm}^{-3}$ is to be expected at growth temperatures near 1400°C, from solvents containing less than 0.1 atom fraction tin.

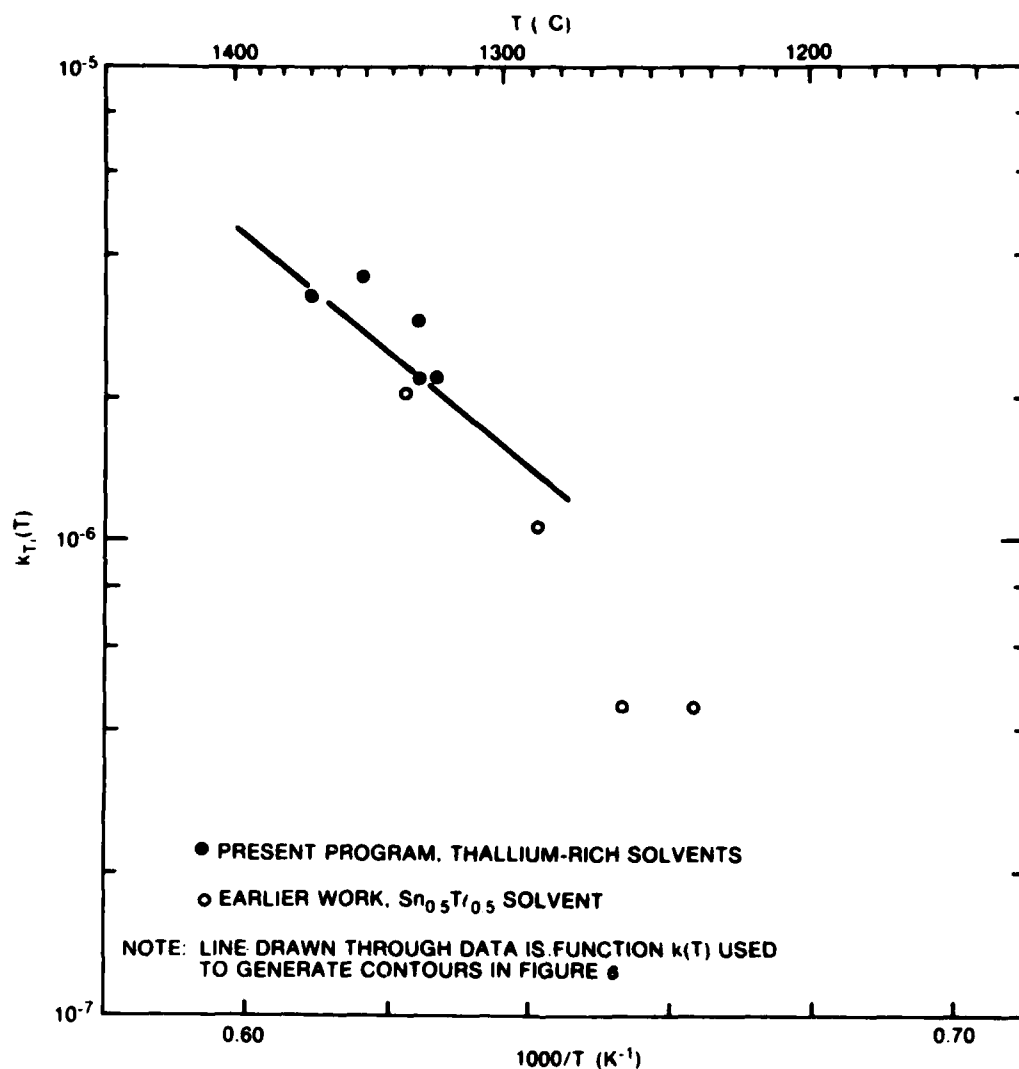


Figure 7. Estimated Values of the Distribution Coefficient for Thallium from Tin-Thallium-Silicon Solutions

It should be pointed out that these calculations do not take into account the possible tendency of the solution at some compositions to segregate into two immiscible liquid phases, one thallium-rich and the other silicon-rich. Within the theoretical framework used to generate Eq. (1), this would be estimated to happen above about 1360°C for a Sn_{0.4}Tl_{0.6} solvent and above about 1380°C for a pure

Tl solvent. The Tl doping results for samples CS-5 and CS-7, which are anomalously high, may be the result of this kind of effect. These estimates are fairly uncertain, though, because the theory is probably not accurate over the wide ranges of solution composition which would occur under solution segregation. Improvement in our knowledge of immiscibility phenomena in the solutions would require experimental determination of the Si-Sn-Tl liquidus at these temperatures.

QUANTUM EFFICIENCY

During the course of optical measurements on several of the solution-grown samples the photoionization absorption of thallium acceptors in the 3 to 5-micron region was observed. The data from sample CS-6 in this region is shown in Figure 8. The continuum absorption in this case reached a maximum value of about 2cm^{-1} at 3200cm^{-1} (3.13 microns). This value corresponds to a maximum theoretical quantum efficiency of roughly 18 percent in a 1-mm-thick detector with antireflection coatings. The measured values from this and other samples are summarized in Table IV. The data are obscured to varying extents by a line at about 3200cm^{-1} , due to frozen water vapor on the samples. Based on the estimated maximum thallium doping value of $2 \times 10^{17}\text{cm}^{-3}$ derived in the previous subsection and the thallium optical cross section of $1.45 \times 10^{17}\text{cm}^2$ deduced here, the maximum theoretical quantum efficiency obtainable in a single pass through a 1mm Si(Tl) detector would be about 25 percent.

TABLE IV. SUMMARY OF QUANTUM EFFICIENCY MEASUREMENTS

Sample No.	Solvent Composition	Growth Temperature	$[Tl]$ (cm^{-3})	$\Delta\alpha$ (cm^{-1} , 3.1 μ)	Quantum Efficiency	Optical Crosssection (cm^2 , 3.1 μ)
CS-6	Tl _{0.86} Sn _{0.14}	1370	1.33×10^{17}	1.95	0.18	1.47×10^{-17}
CS-7	Tl _{0.60} Sn _{0.40}	1330	9×10^{16}	1 ± 0.5	0.1 ± 0.05	--
CS-8	Tl _{0.93} Sn _{0.07}	1325	1.0×10^{17}	1.44	0.13	1.44×10^{-17}
CS-9	Tl _{0.86} Sn _{0.14}	1330	1.2×10^{17}	0.6 ± 0.03	0.06 ± 0.03	--

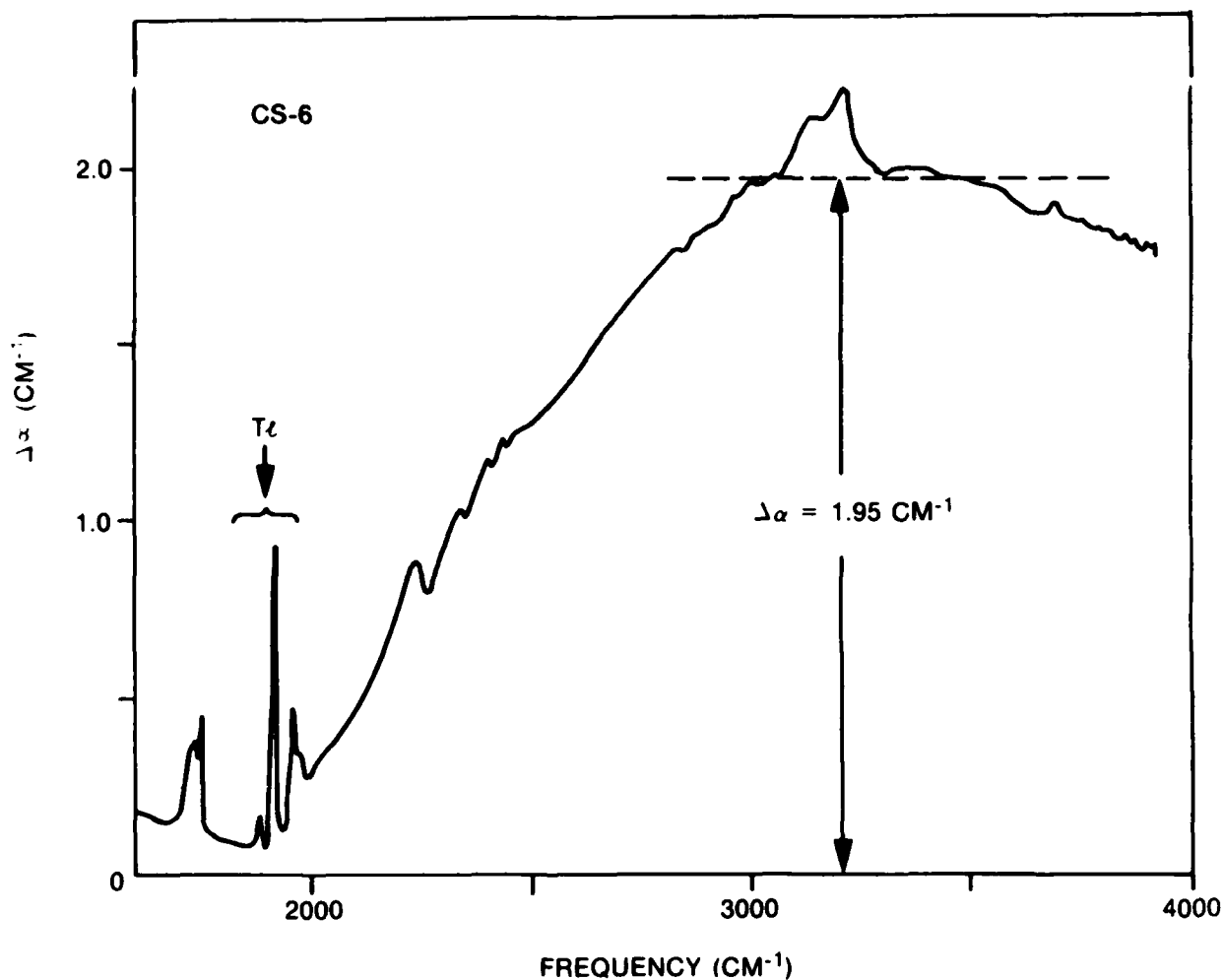


Figure 8. Photoionization Absorption Observed in Sample CS-6

SHALLOW IMPURITIES

As indicated in Table III, various amounts of shallow acceptor impurities were observed in all of the material grown during the program. In some cases the identity of these impurities was determined.

An example of probable boron contamination is illustrated in the Hall data from sample CS-5, shown in Figure 9. Above 250K, the ionization of thallium acceptors is apparent, but at lower tem-

peratures the carrier concentration is determined by the presence of shallower centers. The least-squares fitting program was able to account for the data quite well in terms of thallium and boron acceptors having accepted values of the ionization energy (0.246 eV for thallium, 0.04385 eV for boron). The inferred boron concentration was about $1.9 \times 10^{16} \text{ cm}^{-3}$. When the data was re-fitted allowing the ionization energy of the shallow level to be varied, an optimum value of 0.048 eV was determined, still close to the value for boron.

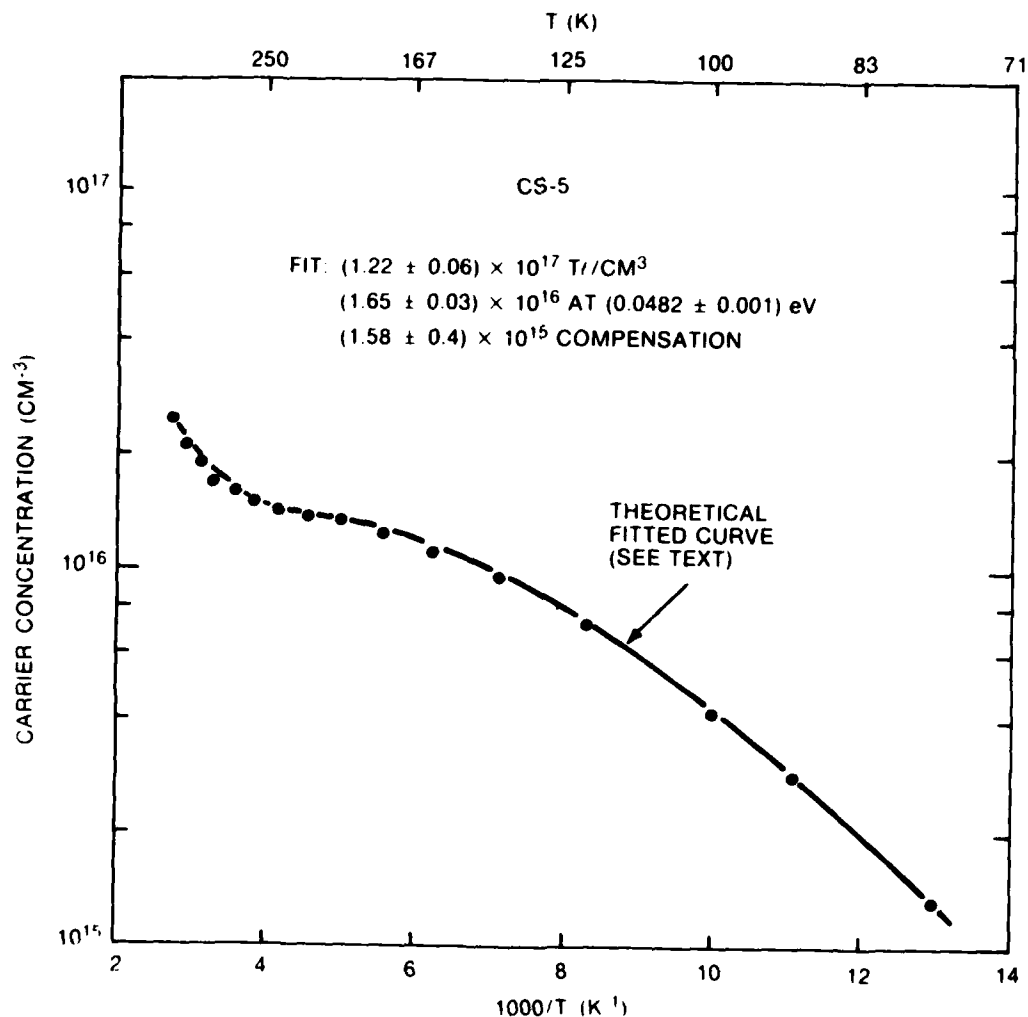


Figure 9. Carrier Concentration Versus Temperature in Sample CS-5

In other Hall data, shallow impurities appeared at somewhat greater ionization energies. An example of this is the Hall data from sample CS-13, shown in Figure 10.

Again the data reveals the characteristic thallium activation energy at high temperatures, but becomes dominated by a second shallower acceptor level below about 200K. A two-acceptor-level fit using the standard thallium and boron ionization energies did relatively poorly in this case, especially in fitting the data below 200K. When the ionization energy of the shallower acceptor was made adjustable in the program, a best-fit value of 0.065 ± 0.002 eV was obtained, considerably deeper than the value for boron and closer to the values for other group IIIA acceptors, aluminum (0.0685 eV) or gallium (0.0722 eV). The shift in this parameter is significant since the fit is greatly improved.

Additional evidence of acceptor impurities deeper than boron appeared in optical absorption data. An example is the absorption spectrum of sample CS-8, shown in Figure 11 over the range $400\text{--}1000\text{cm}^{-1}$. The absorption spectrum of a high-purity silicon reference sample has been subtracted off to eliminate the lattice absorption in this region. Lines which are known to be associated with impurities in silicon are labeled. In addition to substitutional boron, which is responsible for the overall continuum absorption at the low-frequency end of this spectrum and the broad line at 666cm^{-1} , substitutional aluminum is revealed by the line at 469cm^{-1} which corresponds roughly to the aluminum acceptor line at 472cm^{-1} . The intensity of the line corresponds to an aluminum concentration of about $3 \times 10^{14}\text{cm}^{-3}$. In this case no further electrically active impurities were observed, such as gallium (strongest line at 440cm^{-1}) or indium (strongest line at 1175cm^{-1}).

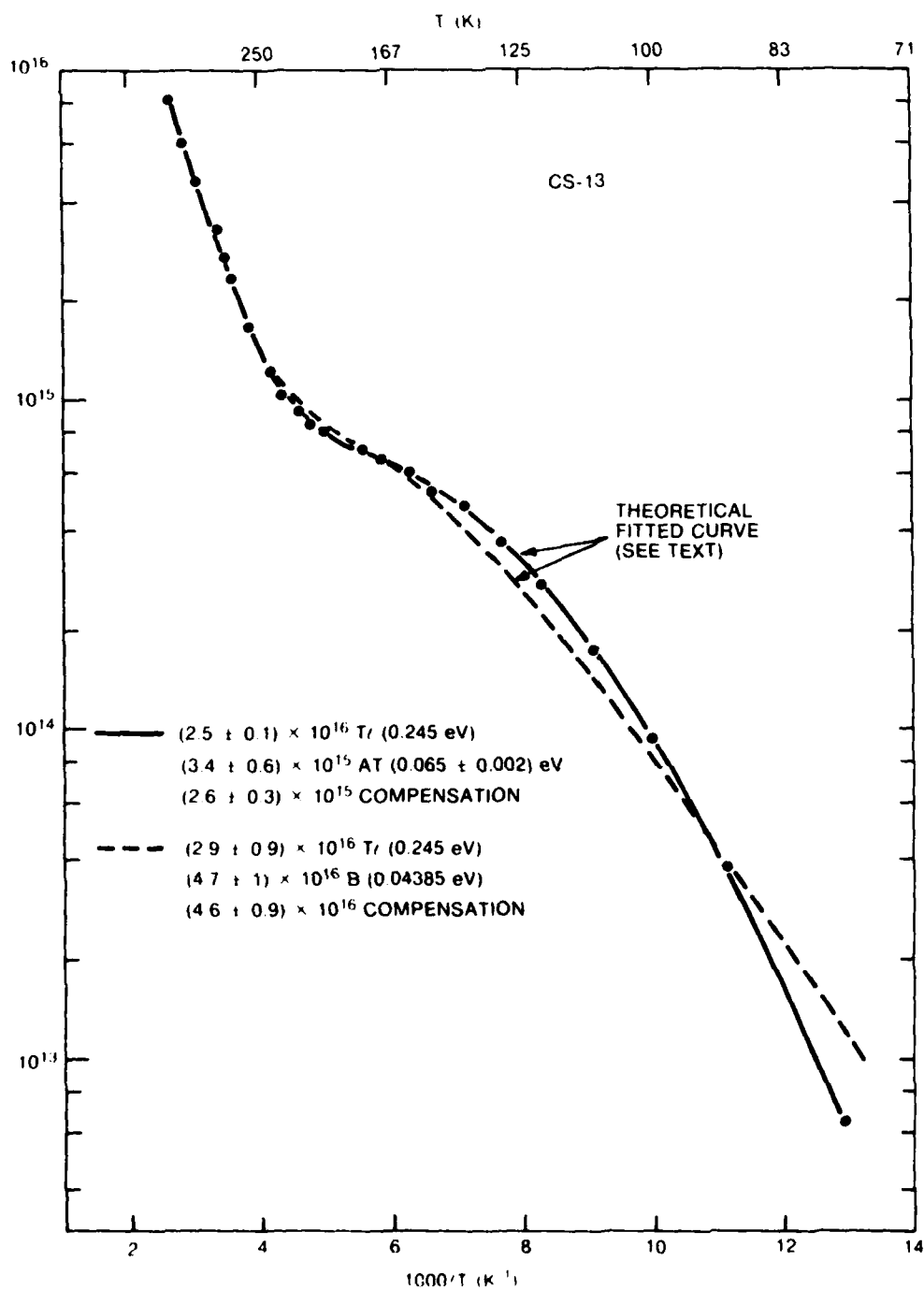


Figure 10. Carrier Concentration Versus Temperature
in Sample CS-13

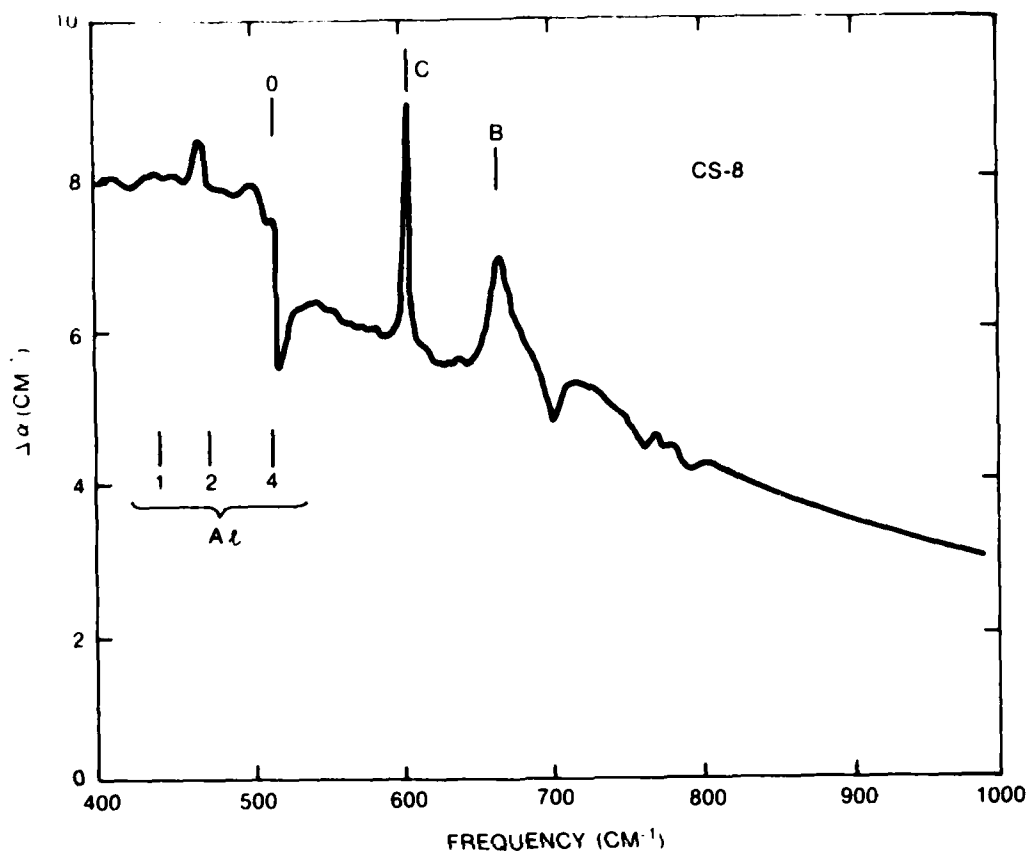


Figure 11. Optical Absorption Spectrum of Sample CS-8 in Region of Several Impurity Absorption Lines

There are several potential factors contributing to the appearance of impurities in the solution-grown material. In the order of occurrence during the growth run, these are:

- 1) Presence of impurities in the starting material
- 2) Introduction of impurities during material preparation and loading
- 3) The presence of impurities in the argon gas used in the crystal growth ampoule
- 4) Evolution of impurities from the container (quartz ampoule) during the growth run.

One very striking phenomenon having implications for the purity of the growth process was the extensive devitrification of the quartz ampoule material (i.e. transformation from an amorphous to a polycrystalline state) during all of the growth runs. At some of the higher growth temperatures used, devitrification initiated on both the inside and outside surfaces of the ampoule, and for longer growth times it extended completely through the ampoule walls, so that an appreciable volume of quartz was involved in a change which may have caused release of impurities.

The manufacturer of the quartz used in the ampoules¹⁰ listed Al_2O_3 and B_2O_3 as typically occurring in concentrations of 50 ppm and 0.5 ppm, respectively, in their material. Such concentrations of these impurities are of an order of magnitude which corresponds to the concentrations seen in the grown material, considering that the distribution coefficient of boron is close to 1 and that of aluminum¹¹ about 0.002.

The changes in the configuration of source, solution and substrate shown in Figure 3 were made as a result of the persistent occurrence of boron in the early crystals. The Suprasil liner shown in the figure was incorporated to reduce the quantity of impurities impinging on the crystal growth materials. The boron content of the Suprasil used¹² was listed as 0 to 0.01 ppm, and that of aluminum 0.1 ppm. The liner consisted of two pieces, a cap and a bottom disc, which were expected to stick lightly to one another at the growth temperature.

The use of the silicon spacer ring and the wetting step described above was intended to further isolate the solution from any impurities penetrating the liner. It was found that during the wetting step the regions of contact between the spacer ring, source and substrate tended to be penetrated with tin-thallium metal

and to fuse together during the subsequent growth runs. This led to what appeared to be total encapsulation of the solution within the silicon parts of the growth assembly.

Analysis of the Hall data on the material grown in these last two runs suggested that the boron was largely removed by these changes, but that lesser amounts (typically around 10^{15} cm^{-3}) of a deeper impurity at around 0.070 eV persisted. It is not clear at present whether this residual effect is still due to contamination external to the growth assembly or to one of the other sources listed above.

Another factor known relatively well is the purity of the various starting materials. The tin and thallium used in the growth runs¹³ were 6 nines grade, specified to have total impurity contents of 1 ppm or less. Such purity limits are more stringent than the specifications on the ampoule material, but are still sufficient to allow boron or aluminum doping in the 10^{15} or 10^{16} range. In view of the low boron levels observed in the encapsulated-solution runs, however, boron levels in the metal are probably negligible at present.

The silicon used in the growth runs varied in purity from Czochralski-grown material with mid- 10^{14} electrically active impurities/ cm^3 to 20,000 ohm-cm float-zone material. All of these concentrations were low enough that they could not account for the concentration of impurities observed after the run.

The other possible contributions to shallow impurities listed above are not known quantitatively, but it seems unlikely that either of these could be the dominant source of electrically active impurities in the growth runs.

The precautions taken during material preparation and handling were typical of those observed in the crystal growth of other semiconductor materials. All of the starting materials were thoroughly degreased and then etched in appropriate acids (1 hour in aqua regia for quartz, 3-5 minutes in CP-4 (five parts nitric acid, one part hydrofluoric acid, one part acetic acid) for silicon, 3-5 minutes in nitric acid for thallium, 3-5 minutes in hydrochloric acid for tin, and 20 minutes in hydrofluoric acid for tin-thallium alloys). Etches involving hydrofluoric acid were always carried out in plastic beakers to avoid pickup of boron from Pyrex glassware. The etches were always quenched with distilled deionized water, followed by 5 minutes or more of additional rinsing.

The argon gas used to fill the ampoule was a grade specified to contain at most 30 ppm impurities. Various sensors used to analyze samples of the gas indicated that the major impurities were oxygen and water vapor.

It is of value to compare the Si(Tl) purity results with past experience in solution growth of Si(In). In the Si(In) case some growth runs were carried out under conditions fairly similar to those used in Si(Tl) growths, using quartz ampoule material from the same source and open (i.e. not encapsulated) indium solutions contained in a well in the silicon substrate. When float-zone purity silicon was used for the growths the shallow impurity concentration was found to be in the low 10^{12} cm^{-3} range, three orders of magnitude down from the Si(Tl) results. The reason for this contrasting result is not definitely known, but again the factors which could account for the difference can be listed.

In general, the temperatures used in the Si(In) growths were somewhat lower (around 1300°C as opposed to 1350°C or higher in some

of the Si(Tl) growths). The quartz ampoules used in the Si(In) growths generally did not devitrify as severely as in the Si(Tl) growths, and never initiated devitrification on the inside surfaces. This may be due to differences in the chemistry and vapor pressures of indium versus the tin-thallium alloy. The vapor pressures of indium and thallium are approximately 3 torr and 400 torr at the respective growth temperatures used. The chemistry of monovalent thallium has in general been found to mimic that of potassium, which has a strong tendency to initiate devitrification of quartz.

Finally, in spite of the fact that the metals used in the Si(Tl) and Si(In) growths were all six nines grade, the species and quantities of impurities present in the indium metal may well have been more favorable for the growth of high purity material.

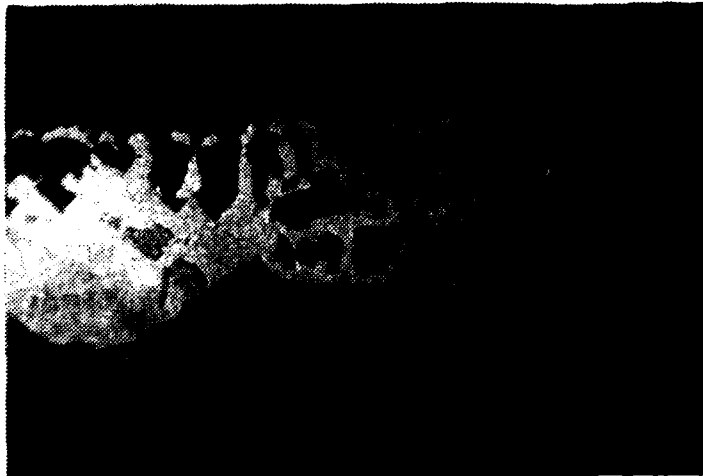
CRYSTAL MORPHOLOGY

The ability to grow reasonably uniform single crystal free of voids and solvent inclusions is a basic prerequisite for further development of thallium-doped silicon detector material. This ability became an issue during the program.

As mentioned in the section on experimental methods, the early growth runs in the program were carried out using a configuration of starting materials in which the solution was rather loosely confined (Figure 3a). The morphology of the crystals grown in this way was adequate for investigating the thallium doping, but was unsuitable for measurements or applications requiring areas of uniform void-free material larger than about 5mm^2 .

Typical growth morphology in these early runs is shown in Figure 12. This is a side view of growth assembly number CS-5 after

being cut open to reveal the solution layer. The original surfaces of the substrate is still partially visible because of spotty wetting of the solution to the substrate. In this particular sampling of the growth morphology, an irregular layer of silicon, between 1 and 1.5mm thick, was deposited on the substrate. Some areas of the substrate were not covered at all. The bottom surface of the source was removed in very irregular fashion, creating "fingers" of the solution projecting up into the source. Slicing the growth assembly parallel to the plane of the solution layer in order to mine out the best portions of the grown material often revealed voids 1 to 2mm in size, spaced a few millimeters apart.



Thickness of solution layer at beginning of run—1mm (magnification 7X)

Figure 12. Growth Morphology Observed at Beginning of Program

The configuration shown in Figure 3b was adopted in growth runs CS-10 through CS-13 in an attempt to improve the morphology of the grown material. The essential changes which were made were to decrease the size of the source-to-substrate gap and to fill the interior volume of the growth assembly entirely with the solution. The motivation for complete filling of the assembly with solution was simply to eliminate bubbles in the solution which would lead to voids in the material.

The rationale behind decreasing the size of the source-to-substrate gap was somewhat more speculative, but was based on existing analyses of the stability of a liquid-solid interface under diffusion-limited growth conditions.¹⁴ In these analyses, stability of a flat growth interface was considered to depend on the relative magnitudes of two competing effects: 1) the tendency of solute transport to be concentrated toward any outward projections in the substrate surface, and 2) the variation in the free energy of the liquid-solid interface with curvature (concave substrate surfaces having lower free energy than convex ones, tending to enhance deposition in recessed areas). The first effect is a destabilizing one in that it tends to exaggerate any nonflatness of the growth interface. The second effect tends to smooth the growth interface, but is more effective for small-scale (short-wavelength) undulations in the growth interface because of the tighter curvature involved for a given amplitude. The net result is that undulations in the growth interface having a wavelength shorter than a certain critical value will tend to be smoothed out while longer wavelength undulations will tend to become more exaggerated. As the solute concentration gradient driving the growth becomes steeper, the region of stability becomes limited to shorter and shorter wavelengths.

In changing the solution growth configuration to incorporate a thinner solution layer, the intent was to discourage sideways diffusion of silicon, thereby putting an upper limit on the scale of wavelengths over which the destabilizing effect could be operative and giving the smoothing effect a greater probability of maintaining a smooth substrate surface. As shown in Figure 13, growth runs carried out under these conditions progressed in a much more stable way than the earlier ones. In this case (growth runs CS-12) a tin-thallium solvent layer approximately 0.1mm thick migrated upwards by about 1.5mm from the original substrate

surface, which is no longer visible. The growth interface remained smooth and the solution layer intact. The grown material was found to be free of voids or solution inclusions.



Thickness of solution layer—0.1mm
(magnification 3X)

Figure 13. Growth Morphology Obtained at
End of Program

The ability to set up such thin solution layers depends on the success of the wetting step described above. To date, the wetting step has been successfully developed only for the tin-thallium alloy composition $\text{Sn}_{0.5}\text{Tl}_{0.5}$ so that the later growth runs were carried out using this composition. The dislocation density was determined in the two samples grown from thin solution layers. The values are summarized in Table V. The results on sample CS-13 indicate that the dislocation density in the grown material is lower than in the substrate from which it was grown. This is surprising but not inconsistent with the conditions of the growth run. Other epitaxial growth processes have been observed to bend dislocation lines out to the edge of the epitaxial material.¹⁵ This is usually associated with some form of stress between the substrate and the

epitaxial material due to slight lattice mismatch. The heavy doping of solution-grown silicon undoubtedly expands the lattice parameter and could generate sufficient lattice mismatch to have such an effect on dislocation lines originating in the substrate.

Table V. Dislocation Densities in
Solution-Grown Si(Tl)

Growth Run No.	Dislocation Density	
	Substrate	Sample
CS-12	--	5000/cm ²
CS-13	40,000/cm ²	8000/cm ²

SECTION IV

CONCLUSIONS AND RECOMMENDATIONS

As summarized in the Introduction, the development of gradient-transport solution growth of thallium-doped solution growth of thallium-doped silicon has been successful on the whole. The growth conditions for high thallium doping have been identified, and an encapsulated-solution technique has been developed which stabilizes the growth process and aids in maintaining the purity of the material grown. The photoionization absorption of the most heavily doped material has been shown to be high enough to provide usable peak quantum efficiencies (up to 25 percent at a 1mm thickness) in detectors. These results indicate that additional development of thallium-doped silicon as a 3 to 5-micron detector material is definitely warranted.

The main areas of this approach which require further work are investigation of detector performance of this material in conjunction with improvements in material purity and crystalline perfection, and scaling up in the rate and diameter of the growth process. With respect to improvement of the material quality, the solution encapsulation technique needs to be developed more fully to include the thallium-rich solvents required for high thallium doping. Once heavily doped crystals of good morphology can be grown in this way, the problem of shallow impurities can be attacked more systematically. The area of greatest uncertainty in the present degree of purity of solution-grown Si(Tl) is the purity of the tin and thallium used.

Purification techniques for these metals may have to be improved to yield silicon crystals capable of optimized detector performance.

In the area of scale-up of the growth process, additional data on the liquidus in the ternary Si-Sn-Tl system would be helpful in understanding the dynamics of the growth process. The growth rate is presently fairly slow, especially for the thallium-rich solvents, and investigation of the upper limits to the growth rate is needed. The growth process needs to be carried out on a somewhat larger scale, so that crystals of larger diameter are produced. The uniformity of the material also needs to be investigated.

Finally, the detector performance of solution-grown Si(Tl) needs to be investigated. As stated in Section 1, the impact on detector performance of material parameters which cannot be controlled easily within the context of this growth process, such as the dislocation density and the presence of incorporated tin, needs to be assessed.

REFERENCES

1. Walter Scott and J.L. Schmit, Appl. Phys. Lett. 33, 294 (1978).
2. C.S. Fuller and J.A. Ditzenberger, J. Appl. Phys., 27, 544 (1956).
3. N. Sclar, interim report on NV&EOL Contract DAAG53-76-C-0209, August 1978.
4. Interim report on NV&EOL Contract DAAG53-76-C-0209, August 1978.
5. M. Hansen, Constitution of Binary Alloys, (McGraw Hill, New York, 1958) p. 1193. See also ref. 7.
6. W.R. Runyan, Silicon Semiconductor Technology (McGraw Hill, New York, 1965) p. 262.
7. C.D. Thurmond and M. Kowalchik, Bell Syst. Tech. J. 39, 169 (1960).
8. O. Kubaschewski and E.L. Evans, Metallurgical Thermochemistry, (Wiley, New York, 1956) pp. 352-353.
9. F.A. Trumbore, C.R. Isenberg and E.M. Porbansky, J. Phys. Chem. Solids 9, 60 (1958).
10. Quartz Scientific, Inc., 819 East St., Fairport Harbor, Ohio 44077.
11. W.R. Runyan, Silicon Semiconductor Technology, (McGraw-Hill, New York, 1965), p. 108.
12. Heraeus-Amersil, Inc., 650 Jernees Mill Road, Sayreville, N.J. 08872.
13. Cominco American, 15128 Euclid Ave., Spokane, Washington 99216.
14. D. Elwell and H.J. Scheel, Crystal Growth From High-Temperature Solutions, (Academic Press, London, 1975) pp. 244-248.
15. G.H. Olsen, J.S. Abrahams, C.J. Buiocchi and T.J. Zamoski, J. Appl. Phys. 46, 1643 (1974).